applied sciences

MDPI

Article

Frost Resistance of Coal Gangue Aggregate Concrete Modified by Steel Fiber and Slag Powder

Daming Luo [1,2], Yan Wang [1,3,*], Shaohui Zhang [2], Ditao Niu [1,2,*] and Zhanping Song [2]

1 State Key Laboratory of Green Building in Western China, Xi'an University of Architecture and Technology, Xi'an 710055, China; dmluo@xauat.edu.cn
2 School of Civil Engineering, Xi'an University of Architecture and Technology, Xi'an 710055, China; zhangshaohui@xauat.edu.cn (S.Z.); songzhpyt@xauat.edu.cn (Z.S.)
3 College of Materials Science and Engineering, Xi'an University of Architecture and Technology, Xi'an 710055, China
* Correspondence: wangyanwjx@126.com (Y.W.); niuditao@163.com (D.N.); Tel.: +86-139-9192-7386 (Y.W.); +86-139-9113-1565 (D.N.)

Received: 26 March 2020; Accepted: 2 May 2020; Published: 6 May 2020

Abstract: Coal gangue, a by-product produced during the process of coal mining and washing, has a serious impact on the environment. Using coal gangue as a concrete aggregate has been proven helpful in potentially improving its value and reducing its environmental impact to a certain extent. However, the high water absorption and low strength of coal gangue aggregate cause a poor frost resistance of coal gangue aggregate concrete (CGAC), and thus limits its application in cold areas. This study attempted to modify the CGAC with steel fibers (including hooked-end, undulated, and copper-plated steel fiber) and slag powder, and investigated its frost resistance. Moreover, the impact that steel fiber and slag powder had on air-void characteristics of CGAC was also analyzed. The results show that when steel fibers were incorporated into CGAC, the compressive strength and splitting tensile strength of CGAC reduced significantly after freezing/thawing and that they experienced the smallest reduction when the content of the steel fiber was 1 vol.% and the undulated steel fibers worked best. However, the effect of slag powder on frost resistance of CGAC at an early age was not obvious, which may be related to the slower pozzolanic reaction of slag powder. Incorporating steel fiber or slag powder into CGAC can optimize its mesostructure and make the air-voids of concrete smaller, which is beneficial to its frost resistance. The results provide a good way to improve the performance of CGAC, expand its application in cold regions, and reduce the pollution caused by coal gangue.

Keywords: coal gangue aggregate; steel fiber; slag powder; frost resistance; pore structures

1. Introduction

Coal gangue, a main solid waste of the coal industry, accounts for almost a quarter of the coal output [1,2]. According to the China National Coal Association (CNCA), the yearly coal output of China has exceeded 3 billion tons in recent years, and the annual increase of coal gangue is more than 400 million tons, resulting in at least 2000 coal gangue piles nationwide [3]. The accumulated coal gangue has been occupying a large amount of cultivated land and its leaching has been causing severe contamination of soil and groundwater [4,5]. At the same time, the coal gangue dust floating in the air infiltrates into the ground with rainwater, which aggravates pollution and seriously affects the lives of residents nearby and the growth of surrounding plants [6,7]. Although many investigations have been conducted on the application of coal gangue in recent years, the utilization of coal gangue is still limited [8–12]. If coal gangue can be made into ceramsite and used as coarse and fine aggregate of

concrete mixtures, the environmental impact caused by both coal gangue and over-exploitation of sand and gravel can be reduced.

In addition, freezing/thawing (F-T) damage is a major cause of durability deterioration of concrete structures in cold regions [13,14], which accounts for almost 60% of China's inland area, where most of the Chinese coal mines exist. However, the poor frost resistance of coal gangue aggregate concrete (CGAC) limits its wide application in cold regions. In recent years, the material properties of coal gangue and the working performance and mechanical failure mechanism of CGAC with aggregate partially or totally replaced by coal gangue have been studied [15–17]. As for the frost resistance of CGAC, the existing research mainly focused on the influences of the content of coal gangue and mineral admixture on frost resistance of concrete [18,19]. However, as a lightweight aggregate, the properties of coal gangue mean that the mechanical properties and durability of CGAC are worse than those of ordinary concrete under the same conditions [20–22]. Since Mangat and Hannat applied the theory of composite mechanics to steel-fiber-reinforced concrete in 1970s [23], the theoretical research and engineering application of steel-fiber-reinforced concrete have developed rapidly [24]. For ordinary concrete, the fibers can significantly enhance the tensile strength, deformation capacity, crack resistance, and durability of concrete [24–29]. Besides, due to the pozzolanic effect and microaggregate filling effect of mineral admixtures, the addition of proper mineral admixtures in concrete can not only save cement but also optimize its pore structure, improve its strength, impermeability, and durability to a certain extent [30–34]. However, there are few studies on CGAC modified by steel fiber and mineral admixture.

This study attempted to replace ordinary crushed stone and river sand with coal gangue ceramsite, modify CGAC with fibers and slag powder, and carry out accelerated F-T testing of CGAC. The frost damage of CGAC was evaluated by compressive strength loss, splitting tensile strength loss, mass loss, and relative dynamic modulus of elasticity (RDME), and the effects of steel fibers and slag powder on the frost resistance of CGAC were studied.

2. Materials and Methods

2.1. Materials

2.1.1. Binding Materials

Ordinary Portland cement (OPC), made by Tangshan Jidong Cement Co., Ltd. (Tangshan, China), was used in this test. Its specific gravity and specific surface are 3.14 and 341 m^2/kg, respectively, and its chemical composition and physical properties are presented in Tables 1 and 2. The physical properties of grade S95 slag powder are provided in Table 3. The water reducing agent used in this study was polycarboxylate superplasticizer with 9% solid content, 25% water reduction rate, and 5.1% air entrainment. The dosage of superplasticizer was 0.6% of the total weight of cementitious materials.

Table 1. Chemical composition of the cement (% wt.).

Chemical Composition	SiO_2	Al_2O_3	CaO	MgO	Fe_2O_3	Na_2O	K_2O	SO_3	Loss on Ignition
Content (%)	20.7	6.16	64.0	1.82	4.41	0.20	1.2	2.6	1.21

Table 2. Physical properties of the cement.

Setting time/min		Flexural Strength (MPa)		Compressive Strength (MPa)	
Initial	Final	3d	28d	3d	28d
100	180	4.5	7.0	27.0	43.6

Table 3. Physical properties of slag powder.

Density (g/cm^3)	Chloride Ion Content (%)	SO_3 (%)	Specific Surface Area (m^2/kg)	MgO Content (%)
3.51	≤0.05	1.5%	435	8.3

2.1.2. Coal Gangue Aggregate

The coal gangue ceramsite shown in Figure 1 was provided by Chaoyang Hualong Co., Ltd. Its physical properties in different particle sizes were measured and are listed in Table 4.

(**a**) (**b**)

Figure 1. Appearance of coal gangue aggregate: (**a**) coarse coal gangue aggregate; (**b**) fine coal gangue aggregate.

Table 4. Physical properties of single-particle gangue.

Particle Size (mm)	0.25~0.50	0.5~1.0	1.0~2.0	3.0~5.0	5.0~10 (Round)	5.0~10 (Gravel)
Bulk density (kg/m^3)	956	834	668	725	680	712
Cylindrical compressive strength (MPa)	21	18	13.7	11.5	7	7.5

2.1.3. Steel Fibers

Three types of steel fibers, namely hooked-end steel fiber (HESF); undulated steel fiber (USF); and copper-plated steel fiber (CPSF) supplied by Sobute New Materials Co., Ltd. (Nanjing, China), were included in order to improve the mechanical properties of CGAC [35,36]. The appearance and properties of the fibers are shown in Figure 2 and Table 5 respectively.

(**a**) (**b**) (**c**)

Figure 2. Appearance of the steel fibers: (**a**) hooked-end steel fiber (HESF); (**b**) undulated steel fiber (USF); (**c**) copper-plated steel fiber (CPSF).

Table 5. Physical properties of steel fibers.

Fibers	Length l (mm)	Diameter d (mm)	Aspect Ratio l/d	Density (g/cm^3)	Tensile Elastic Modulus (GPa)	Tensile Strength (MPa)	Elongation at Break (%)
HESF	30	0.5	60	7.8	475	1457	2.6
USF	30	0.6	50	7.8	248	476	1.8
CPSF	13	0.2	65	7.8	854	3015	3.7

2.2. Specimens Preparation

2.2.1. Mixture Proportions

After adjusting the composition of concrete several times, the mix proportions shown in Table 6 were finally fixed. The content of steel fiber and slag powder had four levels, namely HESF (volume fraction of 0.5%, 1%, 1.5%, 2%), USF (volume fraction of 0.5%, 1%, 1.5%, 2%), CPSF (volume fraction of 0.25%, 0.5%, 0.75%, 1%), and slag powder (mass fraction of 10%, 20%, 30%, 40%).

Table 6. Mixture proportions.

Mixture ID	Component (kg/m^3)					Fiber Volume Fraction (%)			SP (%)	Water Reducing Agent (%)
	Water	Cement	Coarse Coal Gangue Ceramsite		Fine Coal Gangue Ceramsite	CPSF	USF	HESF		
			Gravel	Round						
R0	185	500	400	360	250					0.6
CP0.25	185	500	385.4	344.5	281.1	0.25				0.6
CP0.50	185	500	385.4	344.5	281.1	0.50				0.6
CP0.75	185	500	381.6	341.1	286.9	0.75				0.6
CP1	185	500	379.7	339.4	289.8	1.0				0.6
U0.5	185	500	389.9	349.5	269.7		0.5			0.6
U1	185	500	389.9	349.5	269.7		1.0			0.6
U1.5	185	500	389.9	349.5	269.7		1.5			0.6
U2	185	500	389.9	349.5	269.7		2.0			0.6
HE0.5	185	500	389.9	349.5	269.7			0.5		0.6
HE1	185	500	389.9	349.5	269.7			1.0		0.6
HE1.5	185	500	379.7	339.4	289.8			1.5		0.6
HE2	185	500	369.7	329.3	310.1			2.0		0.6
SP10	185	450	389.9	349.5	269.7				10	0.6
SP20	185	400	389.9	349.5	269.7				20	0.6
SP30	185	350	389.9	349.5	269.7				30	0.6
SP40	185	300	389.9	349.5	269.7				40	0.6

Note: Each mixture was named based on the type of modified materials (R, CP, U, HE, SP = reference group, copper-plated steel fiber, undulated steel fiber, hooked-end steel fiber, slag powder, respectively) and its dosage (0.25, 0.5, 0.75, 1, 1.5, 2 = 0.25%, 0.5%, 0.75%, 1%, 1.5%, 2%, etc., respectively).

2.2.2. Mixing Process

The preparation of CGAC specimens was conducted according to Chinese code GB/T 50081-2002 [37]. The mixing procedures were as follows:

- Mix the fine and coarse aggregate (dry-condition) for 30 s;
- Add steel fibers (HESF, USF, or CPSF) and mix them for 30 s;
- Add cement and mix for 30 s;
- Add the mixing water with superplasticizer into the dry mixture and mix them well for 3 min (with slag powder) or 5 min (with steel fiber).

Finally, the mixture was poured into molds and vibrated for 20 s. After 24 h of curing, the concrete samples were demolded and put in a chamber with a temperature of (20 ± 2) °C and relative humidity above 95%.

2.3. Experimental Methods

2.3.1. F-T Test

The F-T test was performed in accordance with Chinese code GB/T 50082-2009 [38]. The testing procedures were as follows:

- After being cured for 24 days, concrete specimens were taken out of the chamber and soaked in water at about 20 °C for 4 days before the F-T test.
- The specimens were dried, marked, weighed, and then placed them into a rubber box in the F-T chamber. Water was added to the rubber box to about 2 cm above the top of the specimens;
- Temperatures of the center and the surface of the samples were monitored by using embedded temperature sensor.

During the F-T test, the temperature of the cooling chamber and the center of the samples varied from (−18 ± 2) °C to (5 ± 2) °C and from −20 °C to 7 °C, respectively. Every cycle lasted 6 h. After specified F-T cycles, the specimens were wiped dry and the correlative properties were tested. When the RDME dropped to 60% or the mass loss rate reached 5%, the test was stopped.

2.3.2. Evaluation Index of Frost Resistance

(1) Compressive Strength Loss

The compressive strength of 100 × 100 × 100 mm^3 cubic concrete specimens was tested after 100 F-T cycles. The compressive strength loss was calculated by Formula (1) and its end value was the average value of the three tested specimens.

$$Q_c = \frac{f_{c0} - f_{cn}}{f_{c0}} \times 100\% \quad (1)$$

where Q_c is the compressive strength loss of CGAC, %; f_{c0} is the compressive strength before F-T cycles, MPa; and f_{cn} is the compressive strength after n F-T cycles, MPa.

(2) Splitting tensile strength loss

The splitting tensile strength of 100 × 100 × 100 mm^3 cubic concrete specimens was tested after 100 F-T cycles. The splitting tensile strength loss was calculated by Formula (2) and its end value was the average value of the three tested specimens.

$$Q_t = \frac{f_{t0} - f_{tn}}{f_{t0}} \times 100\% \quad (2)$$

where Q_t is the splitting tensile strength loss, %; f_{t0} is the initial splitting tensile strength before F-T cycles, MPa; and f_{tn} is the splitting tensile strength after n F-T cycles, MPa.

(3) Mass loss

The prism concrete specimens of 100 × 100 × 400 mm^3 were used for the mass loss test. After every 25 F-T cycles, the specimens were wiped dry and weighed, and their mass loss was calculated by Formula (3). The average value of the three specimens was taken as the end value.

$$W_n = \frac{m_0 - m_n}{m_0} \times 100\% \quad (3)$$

where W_n is the mass loss, %; m_0 is the initial sample mass, kg; and m_n is the sample mass after n cycles, kg.

(4) RDME

After every 25 F-T cycles, the prism concrete specimens of 100 × 100 × 400 mm^3 were wiped dry and oven dried at 60 °C until the mass was almost constant. The natural frequencies of concrete were measured by using the ultrasonic direct-penetration method (Figure 3) and the RDME was calculated by Formula (4).

$$P = \frac{f_n^2}{f_0^2} \times 100\% \quad (4)$$

where P is the RDME of concrete, %; f_n is the natural frequency of the concrete specimen after n F-T cycles, Hz; and f_0 is the natural frequency before F-T cycles, Hz.

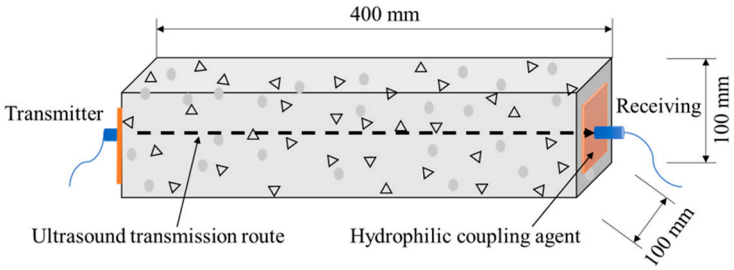

Figure 3. Ultrasonic direct-penetration method.

2.3.3. Air-Void Characteristics before F-T Cycles

Air-void characteristics have a big impact on frost resistance of CGAC [39]. The air-void parameters of CGAC, such as air content, the quantity of voids, mean chord length, specific surface, and spacing factor were graphically examined by using an air void analyzer (Rapid Air 457, Denmark) as shown in Figure 4a.

(**a**) (**b**)

Figure 4. Air-void characteristics test for coal gangue aggregate concrete (CGAC), (**a**) Rapid air concrete air-void analyzer; (**b**) Treated surface of CGAC before air structural testing.

The experiment was carried out according to ASTM C457 [40]. Firstly, the concrete specimen was sliced into surface parallel sections with a size of 100 × 100 × 20 mm and polished with a silicon carbide-glycerol suspension. Then, the polished samples were washed in absolute ethanol by ultrasonic wave and oven dried at 40 °C for 24 h. When they cooled down to room temperature, their polished surfaces were blackened with ink and dried at 60 °C for 30 min. Then, a rubber knife was used to coat zinc oxide evenly on the polished surface (the mass ratio of zinc oxide to Vaseline was 1:3), so that it could be integrated into the air-voids. After the sample cooled down, excess zinc oxide on the surface was scraped off with a rubber knife to make sure only the air-voids were filled with zinc oxide, and the rest of the surface was black, shown as Figure 4b. Finally, the samples were put into a protection box for testing.

Before testing, the sample was placed on the workbench and fixed with screws at both ends. The stepping motor, light and objective lenses were adjusted until the image of the specimen was clearly displayed. The observed area of the sample was 75 × 80 mm^2, and the total length of the observation path was 15,000 mm.

3. Results and Discussion

3.1. Effect of Steel Fiber on Frost Resistance

3.1.1. Compressive Strength Loss

Figure 5 illustrates the impact of the type and content of steel fibers on compressive strength of CGAC before and after F-T cycles. According to the Figure, the mass loss increased rapidly with the increase of freeze-thaw cycles. After 500 freeze-thaw cycles, compared to the R0 mixture with a mass loss of 24.46%, HE1.5 and HE2 mixtures had a mass loss of 27%, while that of HE0.5 and HE 1 were relatively small. The water in the capillary pores of CGAC expanded during its freezing, resulting in formation of microcracks when the expansion force was greater than the tensile strength of the concrete. With the increase of F-T cycles, the microcracks propagated and formed macrocracks, decreasing the concrete strength. In this case, the steel fibers incorporated into CGAC could partially bear the expansion force, which limited the propagation of microcracks, and decreased the strength loss of the concrete. However, the increase of steel fiber content decreased the workability of concrete, and led to steel fiber balling and free water trapping, causing higher air void ratios and more internal defects, thus increasing compressive strength loss of CGAC after F-T cycles [41].

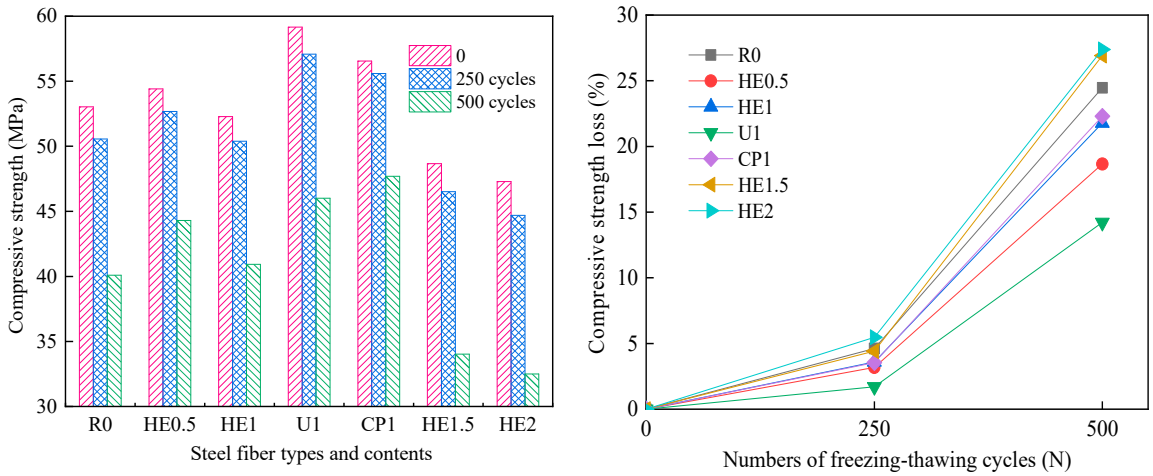

Figure 5. (**a**) Compressive strength and (**b**) compressive strength loss of CGAC reinforced by different types and content of steel fiber after freezing/thawing (F-T) cycles.

For CGAC with 1% steel fiber content, as shown in Figure 5, after 500 F-T cycles, the compressive strength loss of CGAC with 1% USF content was 13.23%, which was the smallest of all the samples. The compressive strength loss of HESF reinforced concrete, CPSF-reinforced concrete, and the reference group were 20.4%, 21.2%, and 24.46%, respectively. It can be seen that, compared with the other two kinds of steel fibers, USF plays a better role in reducing the compressive strength loss.

3.1.2. Splitting Tensile Strength Loss

The splitting tensile strength loss of CGAC with different types and content of steel fibers after F-T is presented in Figure 6. Similar to the compressive strength loss, the splitting tensile strength loss of steel-fiber-reinforced CGAC and the reference group R0 were approximately the same after 250 F-T cycles, ranging from 9% to 13%. After 500 F-T cycles, when the steel fiber content was lower

than 1 vol.%, the splitting tensile strength loss of CGAC decreased with the increase of steel fiber content; and it reached the lowest value of 16.4% when the steel fiber content was 1 vol.%. When the fiber content exceeded 1 vol.%, the splitting tensile strength loss of CGAC increased accordingly, and it reached 24.4% when the fiber content was 2 vol.%. This is because when the steel fiber content is lower than 1 vol.%, most of the fibers can bond well with the cement matrix. When the specimens were subjected to splitting tension, frost damage occurs inside the concrete, but incorporating an appropriate amount of steel fibers has a positive effect on dispersing the stress concentration at the trailing edge of cracks, withstanding tension, and slowing down the cracking development inside the CGAC specimens [42]. Similar to the compressive strength loss test, with more fibers added, it was difficult for them to be mixed evenly, and even agglomeration appeared, which caused a worse bonding performance between concrete and steel fibers and increased the splitting tensile strength loss of CGAC.

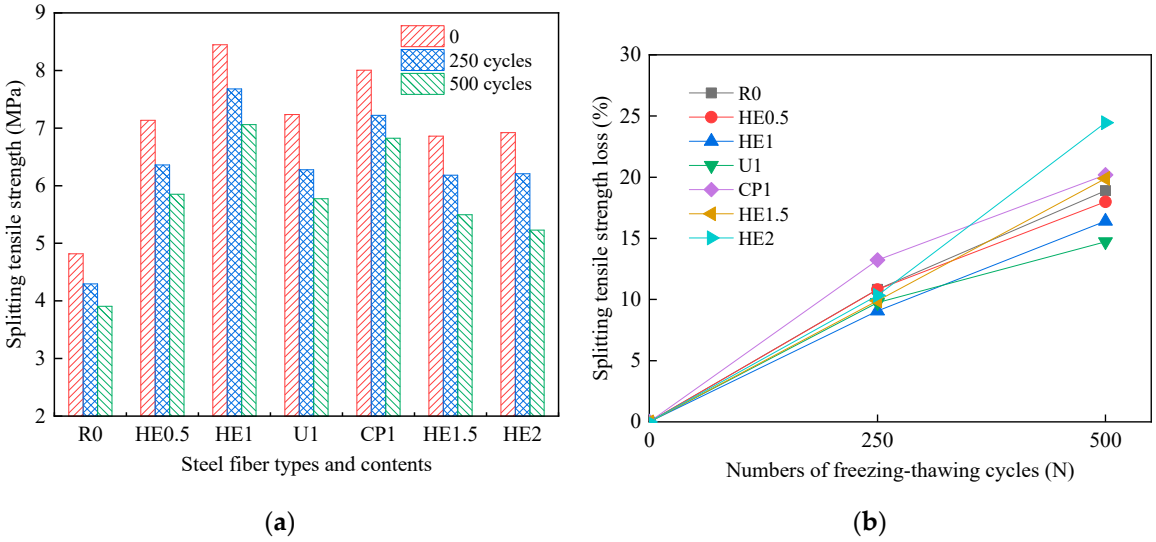

Figure 6. (**a**) Splitting tensile strength and (**b**) splitting tensile strength loss of CGAC with different types and content of steel fibers after F-T cycles.

For 1 vol.% steel-fiber-reinforced CGAC with different steel fiber types, after 500 F-T cycles, the splitting tensile strength loss of USF reinforced CGAC was 14.7%, followed by HESF reinforced CGAC with a splitting strength loss of 16.4%. However, the splitting tensile strength loss of CPSF-reinforced CGAC was larger than that of the reference group. The reason may be that the 1 vol.% CPSF became agglomerations during mixing process, which made the fibers difficult to disperse uniformly and so they could not play an effective role in tensile reinforcement. This was consistent with the experimental phenomenon of poor workability of CPSF-reinforced concrete. Besides, there was not enough cement gel filling in the gap between the agglomerated steel fibers, which resulted in larger pores inside the concrete and increased the damage caused by F-T.

3.1.3. Mass Loss

The mass loss of steel-fiber-reinforced CGAC after the F-T cycles is presented in Figure 7. During the first 100 F-T cycles, the mass loss of CGAC with and without steel fibers increased, which may be caused by the microcracks formed on the surface layer of concrete during F-T cycles. Long time immersion in water made the concrete almost saturate, and the initial frost damage caused little surface spalling, thus increasing the mass of the concrete. After 100 F-T cycles, the mass loss of CGAC decreased. However, the mass of ordinary CGAC decreased the most slowly, and it was even 0.37% higher than the initial weight after 500 F-T cycles. In addition, the steel fiber shape also had significant influence on the frost resistance of concrete. As shown in Figure 7, after the same F-T cycles, the mass loss of ordinary CGAC was less than that of any other steel-fiber-reinforced CGAC, and the mass loss

of CGAC with 1 vol.% CPSF was smaller than that of the other two kinds of concrete, while the mass loss of CGAC with USF was the largest. This was because the coal gangue ceramsite is filled with tiny air-voids, which are similar to the effect of air-entraining agents in ordinary concrete. During the F-T test, the concrete surface layer constantly peeled off, and microcracks gradually formed in the concrete. A large amount of water permeated into the CGAC and ceramsite aggregate, which increased the mass of the concrete.

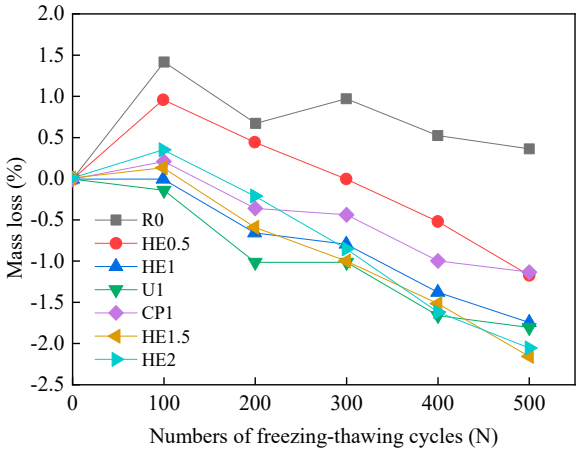

Figure 7. Mass loss of CGAC with different types and content of steel fiber.

Figure 8 shows the surface spalling of concrete after 100 F-T cycles. As can be seen from this Figure, the anti-spalling performance of CGAC without steel fiber is better than that of fiber-reinforced CGAC. With the increase of HESF content, the influence of the steel fiber on mass loss of CGAC became more significant. However, it took at least 500 F-T cycles, which is more than the 300 F-T cycles stipulated by Chinese code, before the surface spalling became obvious [38]. Compared with the other three fiber types, 0.5 vol.% HESF distributed uniformly in concrete and bonded effectively with the paste, thus delaying the surface spalling of concrete. The mass loss of CGAC with 1 vol.%, 1.5 vol.%, and 2 vol.% steel fiber were very close, which indicates that the effect of increasing steel fiber content is limited, instead, the construction cost increases. For CGAC with the same steel fiber content, the surface spalling of CGAC with 1 vol.% USF was much more serious than that of the other two kinds of concrete, while the mass loss of CGAC with CPSF was the largest. This is consistent with the mass loss test results of CGAC in this study, as presented in Figure 7.

(**a**) R0 (**b**) HE0.5 (**c**) HE1 (**d**) U1 (**e**) CP1 (**f**) HE1.5 (**g**) HE2

Figure 8. Surface damage of steel-fiber-reinforced CGAC.

3.1.4. RDME

The effect of steel fiber content on the RDME of CGAC is shown in Figure 9. It can be seen that the RDME of CGAC without steel fibers decreased sharply when F-T cycles increased, while the RDME of fiber-reinforced CGAC increased greatly with the increase of steel fiber content. The RDME of CGAC with 1 vol.% HESF fluctuated greatly, and it reached a maximum of 103.4% after 400 F-T cycles, while that of the CGAC with 1.5 vol.% and 2 vol.% HESF content was relatively stable, fluctuating between 100.0% and 101.9%. Although the performance of the concrete with 0.5 vol.% steel fiber content was better than that of the reference group, the reinforcing effect of steel fiber with this dosage was not as obvious as that of the other three. This may be due to the incorporated steel fiber changing the speed of ultrasound during its transmission in CGAC, causing the increase of the dynamic elastic modulus of concrete [43].

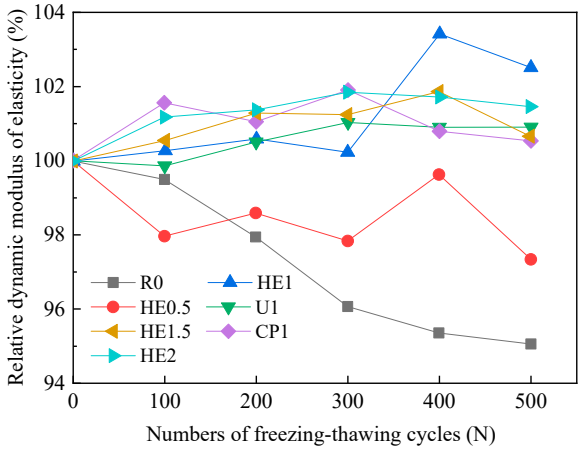

Figure 9. Relative dynamic modulus of elasticity (RDME) of CGAC with different types and content of steel fiber.

For different types of steel fibers, it can be seen from Figure 9 that the RDME of the three kinds of steel-fiber-reinforced concrete with 1 vol.% steel fiber are very close after 500 F-T cycles, and it is higher than that of the ordinary CGAC. This indicates that the bond force, including chemical bond action and the mechanical interlocking of the steel fiber and concrete, can partially bear the internal stress of concrete caused by frost heaving and delay the development of microcracks in CGAC after F-T cycles.

3.2. Effect of Slag Powder

3.2.1. Compressive Strength Loss

Figure 10 demonstrates the compressive strength of CGAC with different slag powder content. It is clear from the Figure that with the increase of slag powder content, the compressive strength of CGAC gradually decreased. Before 250 F-T cycles, the compressive strength of CGAC samples with different slag powder content were very close to each other, but after that, their differences became more obvious. The compressive strength loss of R0 was 24.5%, which was higher than those of SP10 and SP20 (22% and 23.8%, respectively), but lower than those of SP30 and SP40 (25.6% and 29.6%, respectively). Thus, the compressive strength of concrete after F-T cycles was slightly improved by low slag content.

3.2.2. Splitting Tensile Strength Loss

Figure 11 presents the splitting tensile strength of CGAC with different cement substitution rates after F-T cycles. Similar to the compressive strength shown in Figure 10, the splitting tensile strength loss of CGAC specimens grew with the increase of F-T cycles and slag powder content. By the end of 250 F-T cycles, the effect of slag powder content on splitting tensile strength loss of CGAC was

almost the same. After 500 F-T cycles, the differences of splitting tensile strength loss became more remarkable. The splitting tensile strength loss of SP10 was 19.5%, and that of SP40 was 29.1%. The splitting tensile strength loss of the ordinary CGAC was relatively small. Therefore, the slag powder was not conducive to reducing the mechanical strength loss of CGAC when it experienced F-T cycles. This may be because after partially replacing cement with slag powder, the hydration products of cement reduced. Besides, the slag powder was not fully activated at an early age, resulting in less hydration products filling the concrete pores and reducing the frost resistance of concrete [44].

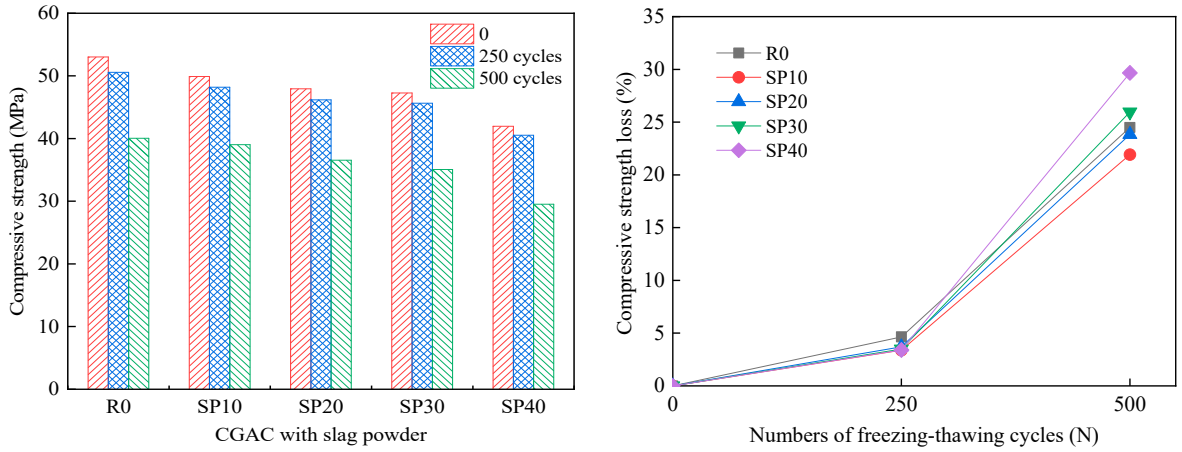

Figure 10. (**a**) Compressive strength and (**b**) compressive strength loss of CGAC with different slag powder content after F-T cycles.

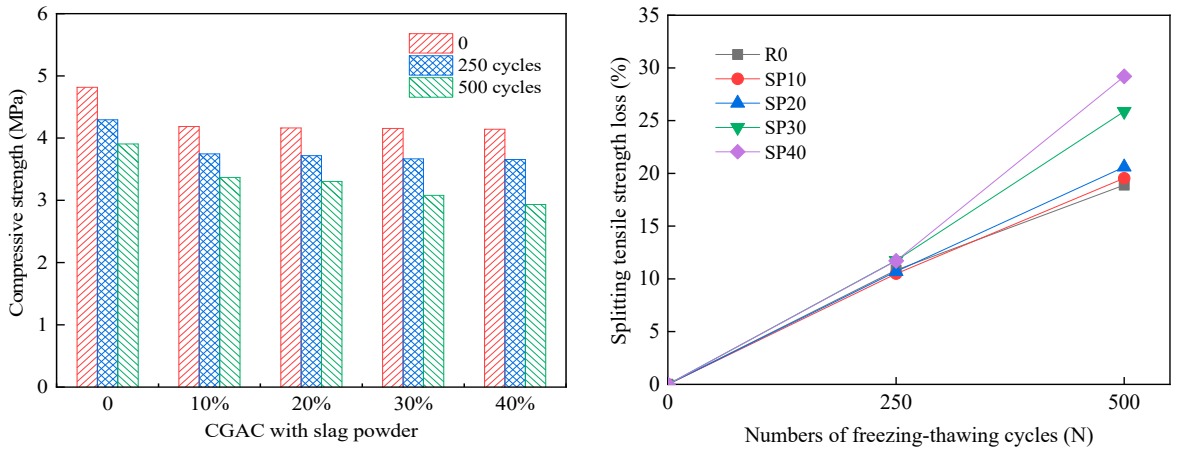

Figure 11. (**a**) Splitting tensile strength and (**b**) splitting tensile strength loss of CGAC with different slag powder content after F-T cycles.

3.2.3. Mass Loss

Figure 12 presents the mass loss of CGAC with different slag powder content after 500 F-T cycles. It is apparent from the Figure that the mass loss of CGAC increased significantly when the cement substitution rate grew, which means the frost resistance of CGAC decreased with the increased substitution rate. However, the mass loss of SP40 was only 1.95% after 300 F-T cycles, and it reached 3.45% after 500 F-T cycles. However, it was still lower than the limit value (5% mass loss) proposed by the Chinese code GB/T 50082-2009 [38].

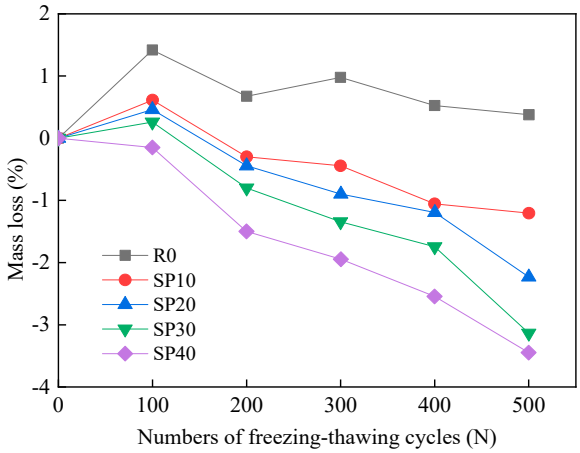

Figure 12. Effect of slag powder content on mass loss of CGAC.

Figure 13 confirms the effect of slag powder content on surface damage of CGAC after 500 F-T cycles. It is obvious that the surface peeling of CGAC with a 40% cement substitution rate was the most serious, which corroborated the mass loss test results. The mass change of ordinary CGAC without slag powder was not significant after 500 F-T cycles. Therefore, the frost resistance of ordinary CGAC cannot be accurately evaluated by the mass loss.

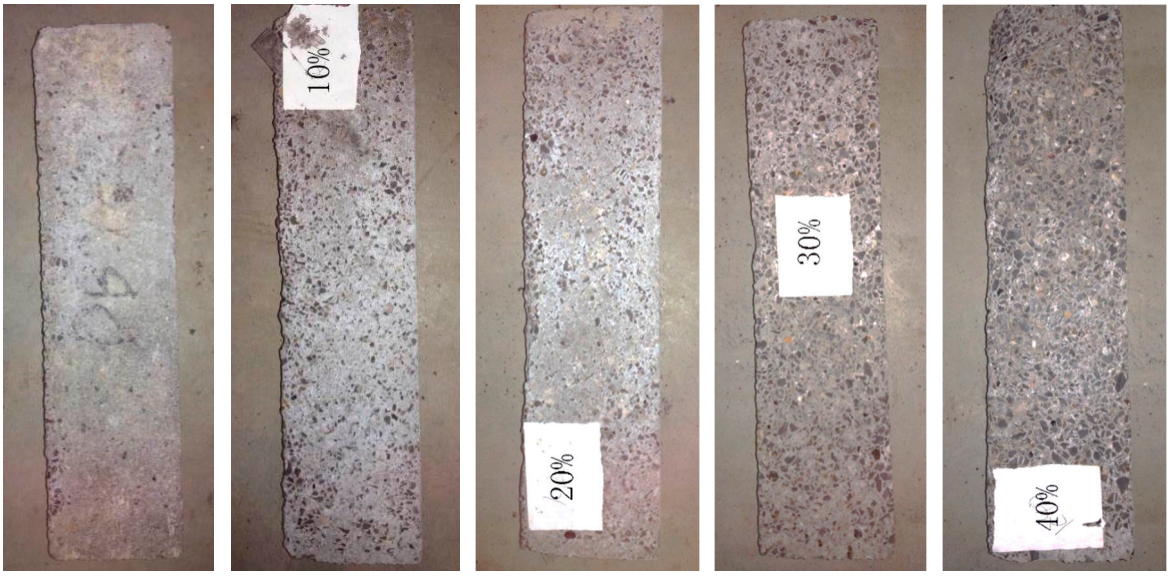

(**a**) (**b**) (**c**) (**d**) (**e**)

Figure 13. Surface damage of steel-fiber-reinforced CGAC after 500 F-T cycles, the cement substitution rates are: (**a**) 0%; (**b**) 10%; (**c**) 20%; (**d**) 30% and (**e**) 40%.

3.2.4. RDME

The effect of slag powder content on RDME of CGAC is shown in Figure 14. In this Figure there is a clear trend that the RDME of CGAC decreased gradually with the increased cement substitution rate after F-T cycles. The RDME of SP10 was close to that of the ordinary CGAC. When the cement substitution rate reached 40%, its effect on frost resistance of CGAC was the most significant, and the RDME decreased the most. However, the dynamic elastic modulus was still more than 90.5% of its original value even after 500 freeze-thaw cycles. That is, the substitution of slag powder for cement did not reduce the frost resistance of concrete very much, which is consistent with the strength loss and mass loss test results.

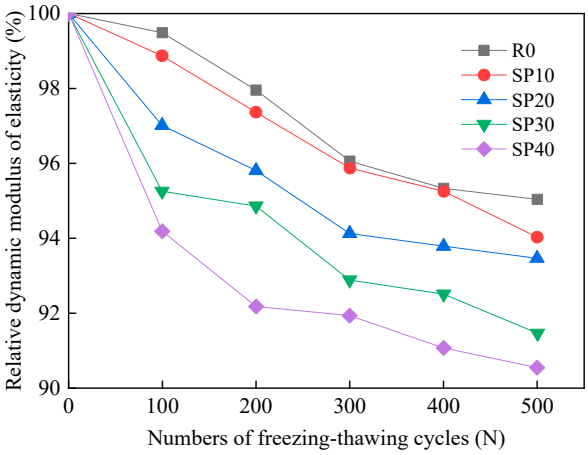

Figure 14. Effect of slag powder content on RDME of CGAC.

3.3. Air-Void Characteristics before F-T Test

To further investigate the improvement of steel fiber and slag powder, the air-void characteristics of CGAC were tested in this study.

3.3.1. Effect of Steel Fiber Type on Air-Void Structure

The air-void distribution and cross-sectional morphology of CGAC with and without steel fibers are shown in Figure 15. Similar to ordinary concrete, coarse and visible pores of low frequency constitute a high proportion of pore volume, while it was the opposite for fine pores, which is well illustrated in Figure 4b. For ordinary CGAC, most air-voids had a chord length of 0.02–0.1 mm. Air-voids with chord lengths larger than 0.5 mm covered a large volume fraction. Especially for the chord length of 0.5–1.0 mm, the air-void content was up to 0.61%. The air-voids became smaller after incorporating steel fibers and more isolated closed pores were found in the cross-sectional morphology. For CGAC with 1 vol.% HESF, the frequencies of the air-voids with chord lengths of 0.01–0.02 mm and 0.02–0.03 mm were 15.2% and 0.98%, respectively, which were much more than that of the ordinary CGAC. Compared with the air-void size distribution of CGAC with HESF, the CPSF-reinforced CGAC had a smaller proportion of small air-voids. This may be related to the smooth surface and flat shape of CPSF, which makes it better for CPSF to be mixed with the concrete mixture, thus resulting in less air being brought into concrete.

It can be seen from the cross-sectional morphology that as a kind of lightweight aggregate, porous coal gangue aggregate can internally cure the concrete, making the interfacial transition zone denser, but it can also weaken the mechanical properties of concrete. On the other hand, the ordinary CGAC has a large number of coarse pores, and the water in the coarse pores generates pressure on the pore wall of concrete when it freezes, which is harmful to the frost resistance of the concrete. The incorporation of steel fibers can reduce the development of microcracks and the formation of coarse pores, and increase the number of isolated closed pores, which will alleviate the expansion pressure caused by water freezing and improve the frost resistance of concrete.

The characteristic parameters of air-voids in CGAC with different steel fiber types are shown in Table 7. It is easy to see that compared with that of the ordinary CGAC, the spacing factor and the mean chord length of air-voids of CGAC with 1 vol.% HESF declined 19.6% and 17.7%, respectively, and the quantity of voids and specific surface area increased by 27.8% and 9.9%, respectively. Fine closed pores are beneficial to the frost resistance of concrete [45], which also helps explain why the frost resistance of HESF-reinforced CGAC is better than that of CPSF-reinforced CGAC.

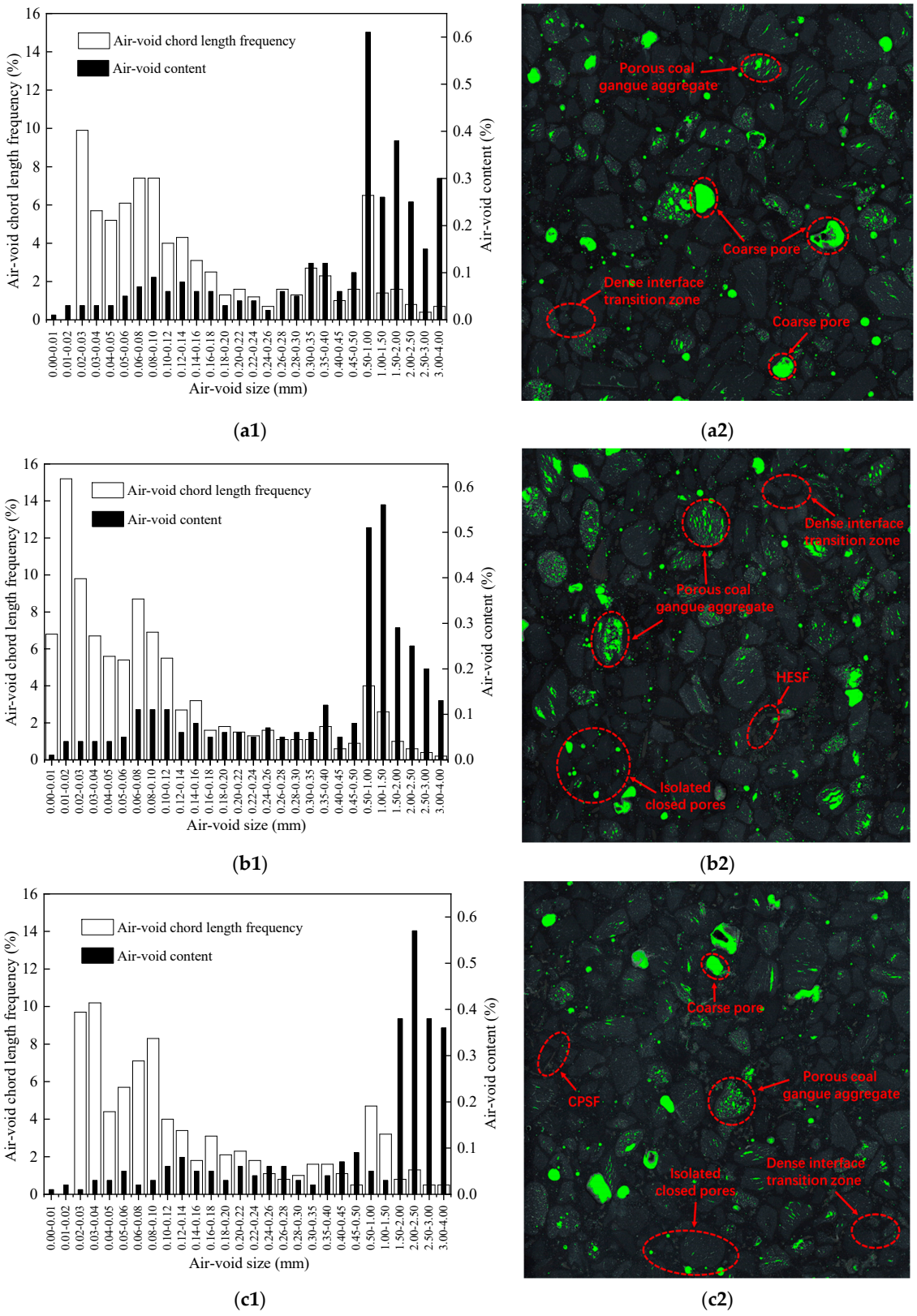

Figure 15. Air-void distribution and cross-sectional morphology of CGAC (**a**) without steel fiber; (**b**) with 1% HESF; (**c**) with 1% CPSF (1: Air-void distribution; 2: Cross-sectional morphology).

Table 7. Air-void characteristic parameters of CGAC with different steel fiber types.

No.	Quantity of Voids	Mean Chord Length (mm)	Air Content (%)	Specific Surface Area (mm^{-1})	Spacing Factor (mm)
CGAC	769	0.232	3.19	17.23	0.367
1 vol.% CPSF	678	0.213	2.54	17.34	0.403
1 vol.% HESF	983	0.191	3.35	18.94	0.295

3.3.2. Effect of Slag Powder Content on Air-Void Structure

Figure 16 illustrates the air-void distribution and cross-sectional morphology of CGAC with different substitution rates of slag powder. After substituting cement with slag powder, the frequency of air-voids with chord lengths of 0.02–0.03 mm decreased, however, the frequency of air-voids with chord lengths of 0.03–0.04 mm and 0.06–0.08 mm increased. For the air-void content, the 0.03–0.04 mm chord length air-voids decreased after incorporating the slag powder. It can also be seen from the cross-sectional morphology that after substituting cement with slag powder, the number of coarse pores reduced and fine isolated closed pores formed due to the filling effect of slag powder. This is beneficial to the frost resistance of CGAC to some extent, but due to the slow pozzolanic reaction of slag at an early age, the improving effect of slag powder on the frost resistance of CGAC is limited. Generally, considering the heterogeneity of CGAC, slag powder cannot effectively optimize its air-void structure, bringing about limited effects on improving its frost resistance.

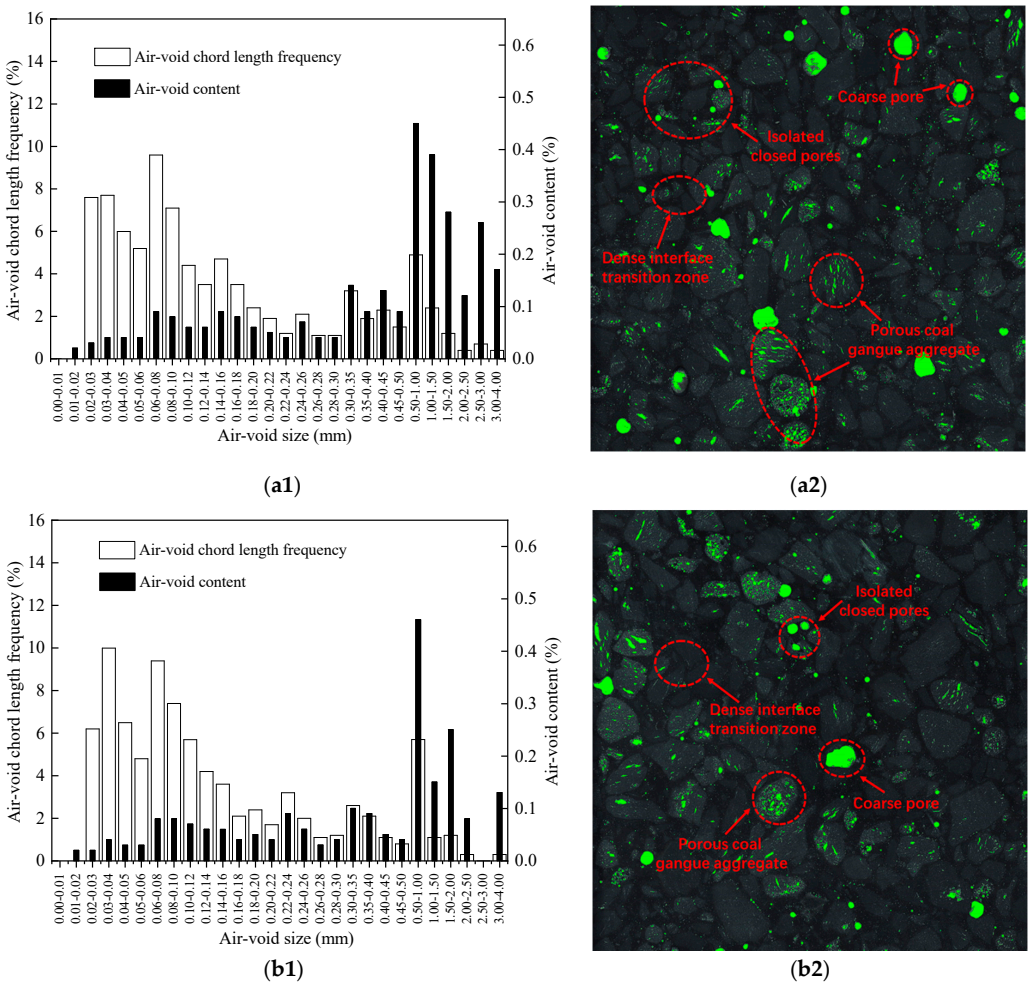

Figure 16. Air-void distribution and cross-sectional morphology of CGAC with (**a**) 10% cement substitution rate; (**b**) 40% cement substitution rate (1: Air-void distribution; 2: Cross-sectional morphology).

The characteristic parameters of air-voids in CGAC with different cement substitution rates are shown in Table 8. It can be seen that compared with that of the ordinary CGAC, the quantity of air-voids and air content of CGAC with 40% slag powder decreased by 13.9% and 30.7%, respectively, and the air-void spacing factor increases by 15.8%, which is entirely consistent with the change of the frost resistance of CGAC with the increase of slag powder content.

Table 8. Air-void characteristic parameters of CGAC with different cement substitution rates.

No.	Quantity of Voids	Mean Chord Length (mm)	Air Content (%)	Specific Surface Area (mm^{-1})	Spacing Factor (mm)
CGAC	769	0.232	3.19	17.23	0.367
10% slag powder	751	0.228	3.06	17.54	0.367
40% slag powder	662	0.257	2.21	21.36	0.425

4. Conclusions

In this paper, the recycled coal gangue was used as concrete aggregate, and the improvements of steel fibers (with different types and content) and slag powder (with different content) on the frost resistance of CGAC were studied. The following conclusions can be drawn from the presented investigation:

- After adding proper types and amounts of steel fibers, the compressive strength loss and splitting tensile strength loss of CGAC reduced, which was beneficial to its frost resistance. However, the mass loss of CGAC increased. Compared with other mix proportions, CGAC with 1 vol.% USF suffered the smallest compressive strength loss and splitting tensile strength loss, with values of 14.2% and 14.7%, respectively.
- The RDME of steel-fiber-reinforced CGAC fluctuated between 100.0% and 103.4% after the F-T test when the content of steel fiber was no less than 1 vol.%, which may be due to the speed change of ultrasound in CGAC or other factors. Thus, the RDME tested by the ultrasonic method may not be suitable to evaluate the frost resistance of steel-fiber-reinforced CGAC.
- The effect of slag powder on frost resistance of CGAC at an early age was not obvious. This may be due to the slow pozzolanic reaction of slag powder and less hydration products filling the concrete pores, as the cement was partially replaced by unactivated slag powder.
- The addition of HESF can obviously optimize the internal structure of CGAC. Just 1 vol.% HESF can increase the quantity and specific surface area of air-voids by 27.8% and 9.9%, respectively, and decrease the spacing factor and mean chord length of air-voids by 19.6% and 17.7%, respectively, thus improving the frost resistance of steel-fiber-reinforced CGAC. However, the slag powder cannot effectively optimize the air-voids structure of CGAC at an early age.

In summary, the replacement of aggregate with coal gangue will reduce both the use of natural aggregate and the impact of solid waste on the environment. Meanwhile, the incorporation of steel fibers can improve the frost resistance of CGAC, optimize its air-void structure, and reduce the mechanical degradation of CGAC caused by frost damage. Besides, replacing partial cement with slag powder can provide a feasible and effective approach to the utilization of such industrial waste without reducing the performance of concrete too much. This study provides a reasonable prospect for the CGAC to be widely used in cold regions.

Author Contributions: Conceptualization, D.L. and Y.W.; Methodology, D.L. and Y.W.; Validation, D.L. and Y.W.; Formal analysis, D.L. and S.Z.; Investigation, S.Z.; Resources, D.N. and Z.S.; Data curation, D.L., Y.W., and S.Z.; Writing—original draft preparation, D.L.; Writing—review and editing, D.N. and Z.S.; Supervision, D.N. and Z.S.; Project administration, D.N. and Z.S.; Funding acquisition, D.N. and Z.S. All authors have read and agreed to the published version of the manuscript.

Funding: This work was financially supported by the National Natural Science Foundation of China (Grants No. 51808438, No. 51878549), and the Opening Fund of State Key Laboratory of Green Building in Western China (Grant No. LSKF202002).

Acknowledgments: The work presented herein was conducted in the State Key Laboratory of Green buildings in Western China at Xi'an University of Architecture & Technology. The authors gratefully acknowledge the support that has made this laboratory and its operation possible.

Conflicts of Interest: The authors declare no conflict of interest.

References

1. Liu, K.; Zhang, X.; Chen, Y. Extraction of coal and gangue geometric features with multifractal detrending fluctuation analysis. *Appl. Sci.* **2018**, *8*, 463. [CrossRef]
2. Querol, X.; Izquierdo, M.; Monfort, E.; Álvarez, E.; Font, O.; Moreno, T.; Alastuey, A.; Zhuang, X.; Lu, W.; Wang, Y. Environmental characterization of burnt coal gangue banks at Yangquan, Shanxi Province, China. *Int. J. Coal. Geol.* **2008**, *75*, 93–104. [CrossRef]
3. Yang, J.; Yang, B.; Yu, M. Pressure Study on Pipe Transportation Associated with Cemented Coal Gangue Fly-Ash Backfill Slurry. *Appl. Sci.* **2019**, *9*, 512. [CrossRef]
4. Wang, S.; Luo, K.; Wang, X.; Sun, Y. Estimate of sulfur, arsenic, mercury, fluorine emissions due to spontaneous combustion of coal gangue: An important part of Chinese emission inventories. *Environ. Pollut.* **2016**, *209*, 107–113. [CrossRef] [PubMed]
5. Bian, Z.; Dong, J.; Lei, S.; Leng, H.; Mu, S.; Wang, H. The impact of disposal and treatment of coal mining wastes on environment and farmland. *Environ. Geol.* **2009**, *58*, 625–634. [CrossRef]
6. Zhao, C.; Luo, K. Sulfur, arsenic, fluorine and mercury emissions resulting from coal-washing byproducts: A critical component of China's emission inventory. *Atmos. Environ.* **2017**, *152*, 270–278. [CrossRef]
7. Sun, Y.; Fan, J.; Qin, P.; Niu, H. Pollution extents of organic substances from a coal gangue dump of Jiulong Coal Mine, China. *Environ. Geochem. Health* **2009**, *31*, 81–89. [CrossRef]
8. Jabłońska, B.; Kityk, A.V.; Busch, M.; Huber, P. The structural and surface properties of natural and modified coal gangue. *J. Environ. Manag.* **2017**, *190*, 80–90. [CrossRef]
9. Li, X.; Zhang, Q. Study on Damage Evolution and Resistivity Variation Regularities of Coal Mass under Multi-Stage Loading. *Appl. Sci.* **2019**, *9*, 4124. [CrossRef]
10. Liu, H.; Liu, Z. Recycling utilization patterns of coal mining waste in China. *Resour. Conserv. Recycl.* **2010**, *54*, 1331–1340. [CrossRef]
11. Zhou, C.; Liu, G.; Wu, S.; Lam, P.K.S. The environmental characteristics of usage of coal gangue in bricking-making: A case study at Huainan, China. *Chemosphere* **2014**, *95*, 274–280. [CrossRef] [PubMed]
12. Wang, J.; Qin, Q.; Hu, S.; Wu, K. A concrete material with waste coal gangue and fly ash used for farmland drainage in high groundwater level areas. *J. Clean. Prod.* **2016**, *112*, 631–638. [CrossRef]
13. Colombo, I.G.; Colombo, M.; di Prisco, M. Tensile behavior of textile reinforced concrete subjected to freezing–thawing cycles in un-cracked and cracked regimes. *Cem. Concr. Res.* **2015**, *73*, 169–183. [CrossRef]
14. Vega-Zamanillo, Á.; Juli-Gándara, L.; Calzada-Pérez, M.Á.; Teijón-López-Zuazo, E. Impact of Temperature Changes and Freeze—Thaw Cycles on the Behaviour of Asphalt Concrete Submerged in Water with Sodium Chloride. *Appl. Sci.* **2020**, *10*, 1241. [CrossRef]
15. Li, D.; Song, X.; Gong, C.; Pan, Z. Research on cementitious behavior and mechanism of pozzolanic cement with coal gangue. *Cem. Concr. Res.* **2006**, *36*, 1752–1759. [CrossRef]
16. Zhang, N.; Sun, H.; Liu, X.; Zhang, J. Early-age characteristics of red mud–coal gangue cementitious material. *J. Hazard. Mater.* **2009**, *167*, 927–932. [CrossRef]
17. Yi, C.; Ma, H.; Zhu, H.; Li, W.; Xin, M.; Liu, Y.; Guo, Y. Study on chloride binding capability of coal gangue based cementitious materials. *Constr. Build. Mater.* **2018**, *167*, 649–656. [CrossRef]
18. Guan, X.; Qiu, J.; Pan, D.; Zheng, J.; Wang, M. Research on the evaluation method of damage degree of coal gangue concrete under freezing-thawing. *Mater. Rev.* **2018**, *32*, 2553–3546.
19. Zhang, J.; Chen, W.; Jin, S.; Chen, C.; Yang, R. Investigation on durability of coal gangue aggregate concrete. *J. Beijing Univ. Technol.* **2011**, *37*, 116–125.
20. Dong, Z.; Xia, J.; Fan, C.; Cao, J. Activity of calcined coal gangue fine aggregate and its effect on the mechanical behavior of cement mortar. *Constr. Build. Mater.* **2015**, *100*, 63–69. [CrossRef]
21. Li, Y.; Yao, Y.; Liu, X.; Sun, H.; Ni, W. Improvement on pozzolanic reactivity of coal gangue by integrated thermal and chemical activation. *Fuel* **2013**, *109*, 527–533. [CrossRef]

22. Karagöl, F.; Yegin, Y.; Polat, R.; Benli, A.; Demirboğa, R. The influence of lightweight aggregate, freezing–thawing procedure and air entraining agent on freezing–thawing damage. *Struct. Concr.* **2018**, *19*, 1328–1340. [CrossRef]
23. Hanant, D.J. *Fiber Cement and Fiber Concrete*; China Architecture & Building Press: Beijing, China, 1986.
24. Marcos-Meson, V.; Michel, A.; Solgaard, A.; Fischer, G.; Edvardsen, C.; Skovhus, T.L. Corrosion resistance of steel fibre reinforced concrete—A literature review. *Cem. Concr. Res.* **2018**, *103*, 1–20. [CrossRef]
25. Park, S.H.; Kim, D.J.; Ryu, G.S.; Koh, K.T. Tensile behavior of ultra high performance hybrid fiber reinforced concrete. *Cem. Concr. Compos.* **2012**, *34*, 172–184. [CrossRef]
26. Monetti, D.H.; Llano-Torre, A.; Torrijos, M.C.; Giaccio, G.; Zerbino, R.; Martí-Vargas, J.R.; Serna, P. Long-term behavior of cracked fiber reinforced concrete under service conditions. *Constr. Build. Mater.* **2019**, *196*, 649–658. [CrossRef]
27. Thomas, J.; Ramaswamy, A. Mechanical properties of steel fiber-reinforced concrete. *J. Mater. Civil. Eng.* **2007**, *19*, 385–392. [CrossRef]
28. Banthia, N.; Gupta, R. Influence of polypropylene fiber geometry on plastic shrinkage cracking in concrete. *Cem. Concr. Res.* **2006**, *36*, 1263–1267. [CrossRef]
29. Teng, S.; Afroughsabet, V.; Ostertag, C.P. Flexural behavior and durability properties of high performance hybrid-fiber-reinforced concrete. *Constr. Build. Mater.* **2018**, *182*, 504–515. [CrossRef]
30. Gruyaert, E.; Van den Heede, P.; De Belie, N. Carbonation of slag concrete: Effect of the cement replacement level and curing on the carbonation coefficient–Effect of carbonation on the pore structure. *Cem. Concr. Compos.* **2013**, *35*, 39–48. [CrossRef]
31. Rostami, M.; Behfarnia, K. The effect of silica fume on durability of alkali activated slag concrete. *Constr. Build. Mater.* **2017**, *134*, 262–268. [CrossRef]
32. Lübeck, A.; Gastaldini, A.; Barin, D.S.; Siqueira, H.C. Compressive strength and electrical properties of concrete with white Portland cement and blast-furnace slag. *Cem. Concr. Compos.* **2012**, *34*, 392–399. [CrossRef]
33. Law, D.W.; Adam, A.A.; Molyneaux, T.K.; Patnaikuni, I. Durability assessment of alkali activated slag (AAS) concrete. *Mater. Struct.* **2012**, *45*, 1425–1437. [CrossRef]
34. Puertas, F.; González-Fonteboa, B.; González-Taboada, I.; Alonso, M.M.; Torres-Carrasco, M.; Rojo, G.; Martínez-Abella, F. Alkali-activated slag concrete: Fresh and hardened behaviour. *Cem. Concr. Compos.* **2018**, *85*, 22–31. [CrossRef]
35. Lee, S.; Oh, J.; Cho, J. Compressive Behavior of Fiber-Reinforced Concrete with End-Hooked Steel Fibers. *Materials* **2015**, *8*, 1442–1458. [CrossRef]
36. Soulioti, D.V.; Barkoula, N.; Koutsianopoulos, F.; Charalambakis, N.; Matikas, T.E. The effect of fibre chemical treatment on the steel fibre/cementitious matrix interface. *Constr. Build. Mater.* **2013**, *40*, 77–83. [CrossRef]
37. Ministry of Construction of the PRC. *Gb/T 50081-2002, Standard Test Method for Mechanical Properties on Ordinary Concrete*; China, M.O.C.O.; China Architecture & Building Press: Beijing, China, 2002.
38. Ministry of Construction of the PRC. *Gb/T 50082-2009, Standard for Test Methods of Long-Term Performance and Durability of Ordinary Concrete*; Ministry of Construction of the People's Republic of China; China Architecture & Building Press: Beijing, China, 2009.
39. Zhang, Y.; Yu, H.; Wang, J. Effect of air-bubble characteristics on salt frost resistance of concrete. *J. Archit. Civ. Eng.* **2011**, *28*, 83–87.
40. ASTM International. *ASTM C457/C457M-16, Standard Test. Method for Microscopical Determination of Parameters of the Air-Void System in Hardened Concrete*; ASTM International: West Conshohocken, PA, USA, 2016.
41. Sivakumar, A.; Santhanam, M. A quantitative study on the plastic shrinkage cracking in high strength hybrid fibre reinforced concrete. *Cem. Concr. Compos.* **2007**, *29*, 575–581. [CrossRef]
42. Yoo, D.; Banthia, N. Mechanical properties of ultra-high-performance fiber-reinforced concrete: A review. *Cem. Concr. Compos.* **2016**, *73*, 267–280. [CrossRef]
43. Acebes, M.; Molero, M.; Segura, I.; Moragues, A.; Hernándezb, M.G. Study of the influence of microstructural parameters on the ultrasonic velocity in steel–fiber-reinforced cementitious materials. *Constr. Build. Mater.* **2011**, *25*, 3066–3072. [CrossRef]

44. Schöler, A.; Lothenbach, B.; Winnefeld, F.; Zajac, M. Hydration of quaternary Portland cement blends containing blast-furnace slag, siliceous fly ash and limestone powder. *Cem. Concr. Compos.* **2015**, *55*, 374–382. [CrossRef]
45. Hasholt, M.T.; Christensen, K.U.; Pade, C. Frost resistance of concrete with high contents of fly ash-A study on how hollow fly ash particles distort the air void analysis. *Cem. Concr. Res.* **2019**, *119*, 102–112. [CrossRef]